2D FRACTAL FLOW GENERATED BY ELECTROMAGNETIC FORCING: LABORATORY EXPERIMENTS AND NUMERICAL SIMULATIONS

Lionel Rossi, Erwan Hascoët, John Christos Vassilicos
Department of Aeronautics,
Imperial College London
London, SW7 2AZ, United Kingdom
l.rossi@imperial.ac.uk, e.hascoet@imperial.ac.uk, j.c.vassilicos@imperial.ac.uk

Yannis Hardalupas
Department of Mechanical Engineering,
Imperial College London
London, SW7 2AZ, United Kingdom
y.hardalupas@imperial.ac.uk

ABSTRACT

Recent works have focused on flow topology and the distribution in space and "size" of the stagnation points. They show that this spatial distribution is closely linked to the energy spectrum and particle pair dispersion statistics. Here we realize flow simulations (laboratory experiments and DNS) where a multi-scale structure of electromagnetically generated stagnation points controls the flow. We thus control the flow's topology and the energy input at each scale. As a first step, we work with a fractal electromagnetic forcing (3 iterations in space) constant in time (step of forcing) of a shallow layer brine flow considered as quasi two dimensional.

- We generate and control a multi-scale "laminar" flow
- Its energy spectrum is $E(k) \sim k^{-p}$ with p=2.5. This is clearly different from small or large scale forcing (p=5/3 or $p \geq 3$) for 2D turbulent flows.
- This exponent (p=2.5) is surprisingly close to theory and shows the possibility to control the energy spectrum by pertinent multi-scale forcing.
- This multi-scale laminar flow presents interesting characteristics for mixing: *i)* during the energy transient, Lagrangian statistics present a ballistic behaviour leading to fluid element pair dispersion statistics with mean square separation $\sim t^{\gamma}$ where $\gamma \approx 3$ as in Richardson diffusion in isotropic turbulent flow. *ii)* After the transient, pair dispersion remains strong. γ is found in the range $2.3 \leq \gamma \leq 2.5$.

INTRODUCTION

Turbulent pair diffusion is intimately linked to concentration fluctuations (Durbin 1980) which are of paramount importance in environmental, geophysical and industrial mixing processes. As documented in Ciofalo (1994), turbulent Prandtl numbers vary over an entire decade to fit data. Lagrangian tracking of fluid element pairs can be used with appropriate synthetic subgrid velocity fields to construct physically viable alternatives to eddy diffusion subgrid models for Large Eddy Simulation (LES), see Flohr and Vassilicos (2000).

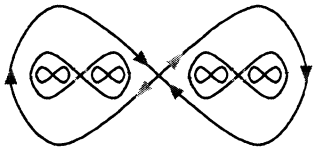

Figure 1: Schematic of a fractal (multi-scale) flow based on a 8 in 8 topology ("cat's eyes" within "cat's eyes").

It is therefore important to understand the physics of turbulent pair diffusion which straddles the entire inertial range of scales. Recent works on the dispersion of fluid element pairs in 2D (d=2) and 3D (d=3) turbulent flows have suggested that the Richardson-Obukhov law (1) is related to the fractal distribution of straining stagnation points in the flow: cf. Fung & Vassilicos (1998), Davila & Vassilicos (2003), Goto & Vassilicos (2004).

$$\frac{\overline{\Delta^2}}{L^2} = G_{\Delta} \left(\frac{tu'}{L} \right)^{\gamma} \tag{1}$$

Δ is the pair separation at time t, L is the outer length scale (characterizing the largest eddies), u' is the rms turbulent velocity, G_{Δ} is the Richardson dimensionless constant and the over-bar represents an average over many pairs and/or realizations.

These works suggest a fractal streamline structure (made of "cat's eyes" within "cat's eyes", see figure 1, in 2D turbulence with an energy spectrum shallower than k^{-3}) and a number of stagnation points, N_s, that scales as (2).

$$N_s = C_s \left(\frac{L_0}{L} \right)^d (L/\eta)^{D_s} \tag{2}$$

L_0 is the size of the system, C_s is a dimensionless constant and the inner length-scale, η, defines, with L, the range of scales where the energy spectrum varies as $E(k) \sim k^{-p}$. The fractal dimension, D_s, is related to p by equation (3) and to γ by $\gamma = 2d/D_s$ (when p=5/3, D_s=4/3 and $\gamma = 3$).

$$2D_s/d + p = 3 \tag{3}$$

To test these ideas in a fully controlled way, we need to create a 2D flow with a streamline structure such as in figure

1, and with the possibility to modify the flow and the fractal dimension, D_s, at will.

We propose to achieve this by fractal electromagnetic forcing. Numerous previous works have used electromagnetic (EM) forcing to generate turbulent quasi two dimensional (Q2D) flow, among them Cardoso et al (1994), Sommeria (1986), Williams et al (1997). Multiple-scale forcing has been applied by Queiros-Conde & Vassilicos (2001), Staicu et al (2003), Hurst & Vassilicos (2004) who used fractal grids in a wind tunnel to stir flows over many scales at once.

Here we combine both approaches to create a multiple-scale fractal EM forcing of a Q2D flow. In addition, the laboratory experiments are complemented by Direct Numerical Simulations (DNS).

LABORATORY EXPERIMENTS AND DIRECT NUMERICAL SIMULATIONS

This section briefly describes the laboratory experiments and the DNS performed.

Laboratory experiments

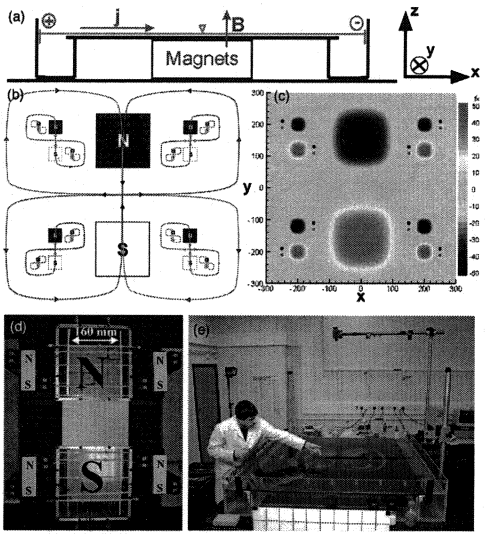

Figure 2: (a) Rig's schematic for electromagnetic forcing of a shallow brine layer, (b) Schematic of a fractal flow and associated permanent magnets, (c) Electromagnetic forcing distribution, I=1A, B_{ref}=1T, f_y in N/m^3 , (d) Under-wall distribution of permanent magnets used in experiments, (e) Photo of the rig.

In the laboratory experiments, electromagnetic body forcing ($\mathbf{j} \times \mathbf{B}$) is produced by the use of permanent magnets ($\mathbf{B}$, Bonded NdFeB, Br 0.68T) placed under the wall and electrical currents ($\mathbf{j}$) generated by platinum electrodes on each side of the tank. EM forcing is used over many scales simultaneously to design the stagnation point distribution of figure 2a. The three scales of forcing are imposed by the magnets' size: 160 mm, 40 mm, 10 mm. This leads to a scale factor of 4 for the fractal forcing, implying $D_s = 0.5$ for the design of figure 2a. The size of the tank (1700x1700 mm) is large compared to the size of the magnets and the EM forcing area of the experiment represents only 2.8% of the total area of the bottom wall which is small compared to all previous works. The thickness of the brine layer (salt water, 158g/l NaCl) is about 5 mm, in which case the flow is as Q2D as possible (Satijn et al 2001) without too much bottom friction which could halt the flow (Clercx et al 2003). In our case the dissipation due to the bottom friction is compensated by the sustained forcing. The kinematic viscosity, ν, is about 1.3 $10^{-6} m^2/s$.

Table 1: Typical scales of the fractal flow according to the forcing intensity. I is the electric current intensity. L_E is the Eulerian integral length scale computed via spatial velocity correlation. $Re_{2D} = u_{rms} L_{PIV}/\nu$ is the "2D" Reynolds number based on the root mean square velocity in the measurement frame

I (A)	u_{rms} (mm/s)	$L_E(mm)$	Re_{2D}
0.1	2.09	158.6	1300
0.15	3.06	162	1900
0.2	3.83	165.1	2300
0.3	5.84	172.2	3600
0.4	7.48	177.8	4600
0.53	9.55	183.1	5900
0.7	12.1	189.3	7400
1	16.1	195.3	9900

The Navier Stokes equation, (4), with gravity and the usual Lorentz body forces $\mathbf{j} \times \mathbf{B}$ term is:

$$\rho \frac{D\mathbf{u}}{Dt} + \nabla P + \rho \mathbf{g} = \mu \nabla^2 \mathbf{u} + \mathbf{j} \times \mathbf{B} \qquad (4)$$

The measurements presented in this paper are based on visualisation.

For dye visualisation a standard digital camera with 3M pixels was used. The main dye used is fluorescein. For multicolor purpose, red and white screen printing ink (water based) were also used.

For PIV measurement, a camera with a resolution of 2048x2048 $pixels^2$ and a dynamic range of 64db 12bit (Kodak MegaPlus Model ES 4.0) was used. The PIV grid is about 287x287 with 56% overlap. The correlation windows (about 6.35mm) are smaller than the small scale of forcing. The maximum (x and y) displacement is about 13 pixels for the searching-windows. The PIV software is an in house software of Mechanical Engineering Department Imperial College London.

Table 1 gives some typical values of the measurements.

Direct Numerical Simulations

In addition to the experiment, we performed DNS of the forced Navier-Stokes equation in a 2D square domain, see equation 5. $f_0\mathbf{f}(\mathbf{r})$ is the Lorentz force, f_0 being the amplitude (in the current experiments f_0 is independent of $\mathbf{r}$) and $\mathbf{f}(\mathbf{r})$ being a unit vector accounting for the spatial distribution of the magnets. The Rayleigh friction term $-\alpha\mathbf{u}$ is added in order to model bottom friction which is the leading dissipation mechanism in a shallow layer flow.

$$\partial_t \mathbf{u} + (\mathbf{u} \cdot \nabla)\mathbf{u} = -\nabla P - \alpha \mathbf{u} + \nu \Delta \mathbf{u} + f_0 \mathbf{f}(\mathbf{r}) \qquad (5)$$

The boundary conditions are periodic, the effect of lateral boundaries being negligible for a domain size ($2\pi \times 2\pi$) large compared to the size of the square magnets ($2\pi/5 \times 2\pi/5$, $2\pi/20 \times 2\pi/20$, $2\pi/80 \times 2\pi/80$). The modified Navier-Stokes equation is integrated with a Fourier pseudo-spectral algorithm on a 1024^2 grid.

TOPOLOGY OF THE FLOW

The study and control of the topological structure of the flow are important as we aim to achieve a multi-scale flow where we control "multi-scale" stagnation points.

Dye visualisations

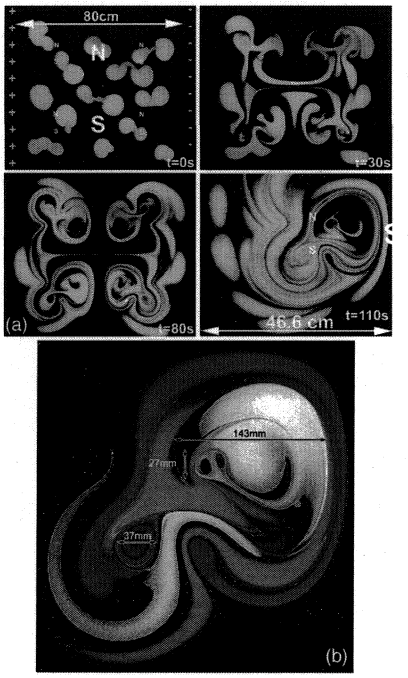

Figure 3: Dye visualisations for I=0.3A, (a) Entire flow, magnets (M160 and M40) are indicated by N and S, while the electrical potential is indicated by + and -. The power is switched ON at t=0, (b) Quarter flow, picture taken about 75s (i.e. $tu_{rms}/L_E = 2.5$) after switched ON.

Figure 3 shows dye (fluorescein) visualisations of the multi-scale flow generated for I=0.3A. The positions of the large and medium sized magnets are indicated in figure 3 by N (North) and S (South). The three scales associated with the forcing are clearly present. The effective generation of stagnation points at different scales and of fractal flow (similar to figure 1) is demonstrated. Figure 3a shows time evolution of the entire flow. After 30s (i.e. $tu_{rms}/L_E = 1$), the visualisation gives some closed flow loops at the small scales of forcing (M_{10}) while the larger scales dye-lines are not yet closed but still strongly defined by the forced stagnation point. These are the different time-scales of flow/forcing associated to the length-scales of forcing. After some time the flow becomes quasi-stationary, keeping its multi-scale topology. Figure 3b shows a quarter of the flow after 75s (i.e. $tu_{rms}/L_E = 2.5$). The large scale of forcing (M_{160}) is on the right of the picture and some characteristic length-scales are given. It is clear that each scale of forcing is closely linked to flow scales and that the controlled stagnation points can be associated to a flow length-scale about the size of the local forcing. Given that, the three scales of magnets/forcing will be generally used as references in our analysis of the multi-scale aspect of the flow. As the initial condition of picture 3b is one blob for each color, the dye on the upper-flow part of the stagnation points is extremely illustrative of the mixing/stirring mechanism associated with these points, as well as the interconnection between the scales.

Particle Image Velocimetry (PIV) and scale analysis

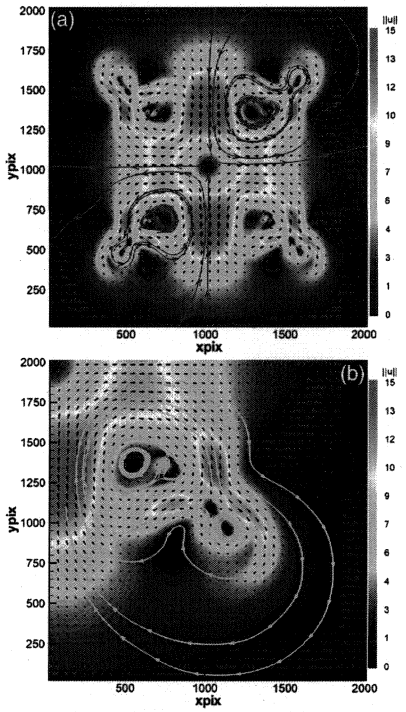

Figure 4: PIV measurements for I=0.3A, (a) entire flow, frame 80cm, (b) quarter of the flow, frame 40cm. 1 arrow out of 8 is represented, $\|\mathbf{u}\|$ in mm/s, x and y in pixels. Some streamlines are given by grey and white lines

Figure 4 presents PIV measurements of the entire flow (frame 80cm, figure a) and a quarter of it (frame 40cm, figure b) for an electrical current of I=0.3A (same as for flow visualisations presented in previous section). The large scale stagnation point controlled by the forcing M160 is clearly well defined. The "8 in 8" flow topology is apparent in the velocity field, with the three iterations linked to the fractal set of magnets. The PIV measurements have sufficient spatial resolution to accurately capture the fractal topology of the velocity field. The maxima of velocity appear above the forcing scales M160 and M40. The fluid flows above magnet-pairs M40 have an a-symmetry due to the coupling with the larger scale of flow/forcing (M160). Nevertheless, the forcing at scale M40 is strong enough to impose stagnation points.

In figure 5 we plot the small scale flow's streamlines extracted from PIV measurements (frame 80cm) for I=0.3A. The topology shows two hyperbolic stagnation points associated to three "vortices". It should be noticed that the small scale flow going up in between the two small vortices is the pumping effect of the south magnet (M_{10}) placed under the wall. The concordance with figure 3 is striking. The topology of the small scale flow does not change across the whole range of flow intensities studied here. The flow topology at small scales is thus controlled by the small scales of the forcing.

The velocity field topology (figure 4 and 5) is in clear agreement with that of the flow visualisation (figure 3). This demonstrates the effective generation of stagnation points at different scales and successful measurement of such a velocity

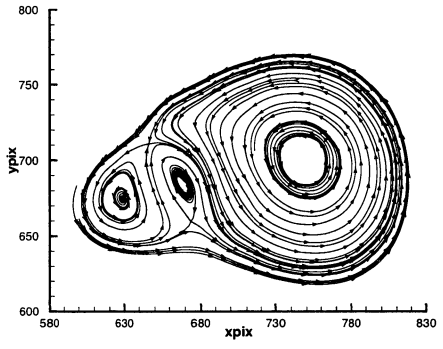

Figure 5: PIV measurements (I=0.3A), streamlines at small scales

field.

Varying the intensity of the electrical current (i.e. forcing) allows us to change the intensity of the flow, without significantly changing the fractal streamline structure of the flow, over more than one order of velocity magnitude.

DNS

The DNS shows good agreement with the laboratory experiment on the distribution of stagnation points and streamline pattern, see figures 3, 4, 6. The slight differences in streamline shapes are due to the fact that the ratio of the size of the box (or tank) over the size of the magnets is twice smaller for the DNS than for the rig.

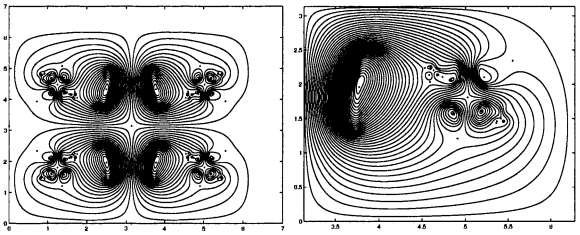

(a) (b)

Figure 6: DNS streamlines pattern and stagnation point location; (a) full flow (b) bottom right quarter

CONTROL OF THE ENERGY SPECTRUM

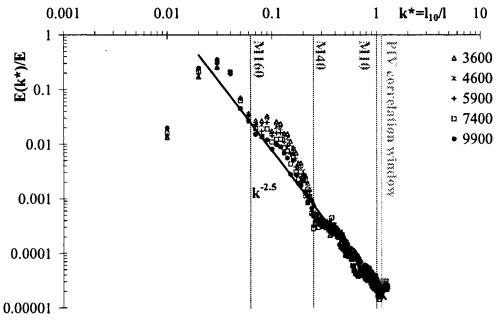

Figure 7: Flow energy spectrum for different values of the Reynolds number Re_{2D}. The 3 sizes of forcing (M_{10}, M_{40}, M_{160}) as well as the PIV correlation window size are indicated by vertical straight lines. Diagonal straight line illustrates $k^{-2.5}$. PIV frame 80cm.

The energy spectra are extracted from the quasi-stationary flows imposed by permanent forcing in time.

As shown in figure 7 and 8, we generate energy spectra $E(k) \sim k^{-p}$ with $p \sim 2.5$ which is different from the 5/3 value obtained when the forcing is purely small scale (inverse cascade of energy) and the value 3 (or higher) obtained when the forcing is purely large scale (direct cascade of energy) in 2D turbulence. Furthermore, the expected exponent of the energy spectrum from the design of figure 2a and $p + D_s = 3$ is about 2.5 which is surprisingly close to the one of the simulations. The oscillations of the energy spectra decrease with the increase of the Reynolds number. They correspond to the spatial periodicity of the forcing.

To our knowledge, this is the first 2D laboratory set up where a power spectrum with a prescribed exponent is imposed and controlled by the forcing.

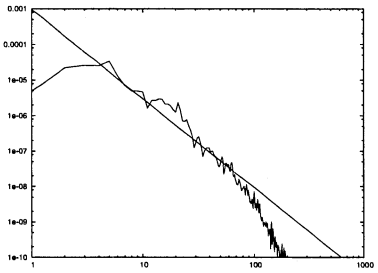

Figure 8: Energy spectrum for DNS, $H_a^2 = f_0^2/\nu\alpha^3 \sim 8\ 10^2$

The good agreement between experiments and DNS confirms that this control comes from the spatial distribution of the forcing and associated stagnation points.

MIXING AND LAGRANGIAN STATISTICS

Figure 9 gives an illustration of the mixing/stretching of 3 initial blobs of different colors. This time-series clearly shows a stretching mechanism where the presence of alternative color "lines" (black, orange, green, white) and very long interfaces are striking. Adding time dependence of the forcing should increase the mixing.

Lagrangian statistics are computed from time resolved PIV measurements by integrating trajectories of fluid elements. To remove the noise at small scales a 3x3 averaging is used taking benefit of the 56% overlap. Even if the main flow is in the measurement area, some fluid elements are moving inside and outside the measurement area. To keep constant the number of fluid elements in our one- and two-particle statistics, the flow is closed at the size of the tank (via continuity equation) to ensure mass conservation. Except for the quality of the statistics, there are no effects on the physics of the flow as: *i)* only the fluid elements crossing the measurement area are taken into account; *ii)* the velocity of the flow outside the measurement area is more than 10 times smaller than u_{rms}, leading to a potential mixing there more than 100 times smaller than the one in the measurement area; *iii)* the turn-over time scale in that outer area is extremely large (100 times) compared to the flow turnover time (L_E/u_{rms}) which is itself larger than the Lagrangian time. *iv)* The duration of the acquisition is kept much smaller (10 times) than the turn-over time in the outer area.

The lagrangian correlation time is $T_L = 28.15s$ (i.e. $T_L = 0.37L_E/u_{rms}$) and is extracted from the lagrangian corre-

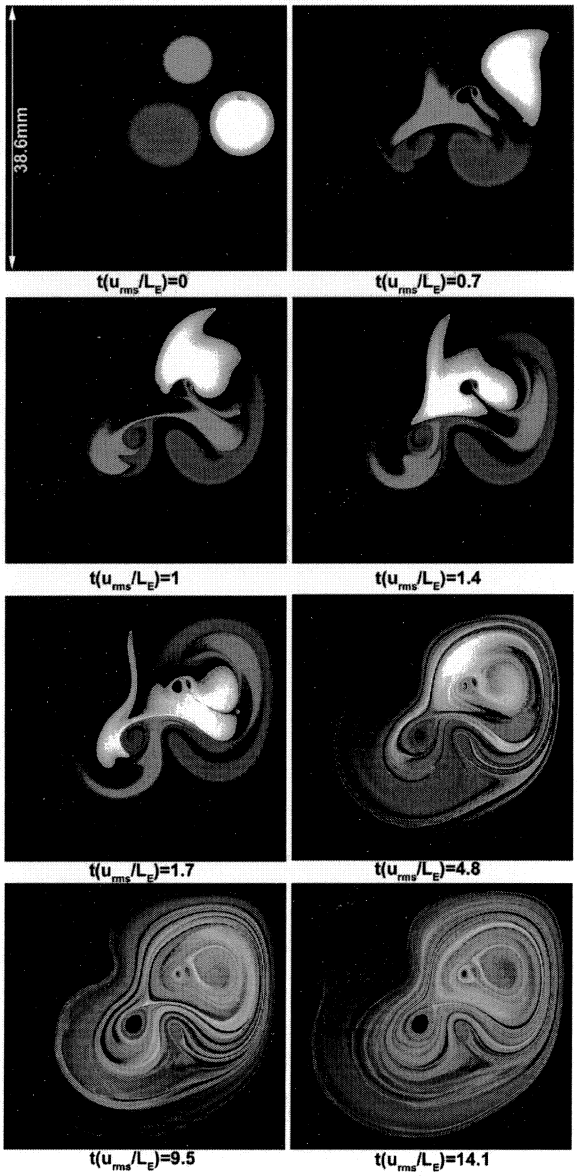

Figure 9: Illustration of dye mixing and stretching with a multi-scale electromagnetic forcing constant in time for a quarter of the flow (I=0.3A).

lation function given in figure 10 for $Re_{2D} = 1300$. The oscillations in the lagrangian correlation are the consequences of the symmetry of the frozen flow and its turn-over times.

Figure 11 (a&b) gives fluid elements pair dispersion with an initial separation of $\Delta_0 = 1$ *pixel*. The sensitivity to Δ_0, for short times, has recently been noted, Nicolleau & Vassilicos (2003), Flohr & Vassilicos (2000). In addition, figure 11b gives the derivative (linear estimation) of the dispersion which is less sensitive to Δ_0. These two curves show two different values of γ (6): $\gamma = 3.1$ between switch on and end of transient (estimated from energy growth) and $\gamma = 2.3$ for longer times.

$$\frac{\overline{\Delta^2}}{L_E^2} = G_\Delta \left(\frac{t}{T_L}\right)^\gamma \qquad (6)$$

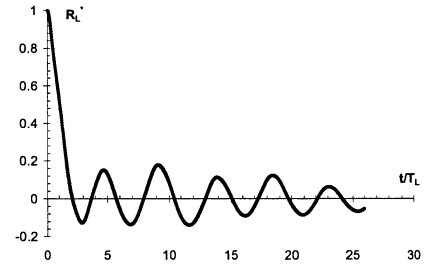

Figure 10: Dimensionless Lagrangian correlation, R_L^*, versus dimensionless time, t/T_L. $R_L(\Delta t) = \frac{1}{N_t}\sum_t < \mathbf{u}(t) \cdot \mathbf{u}(t + \Delta t) >$

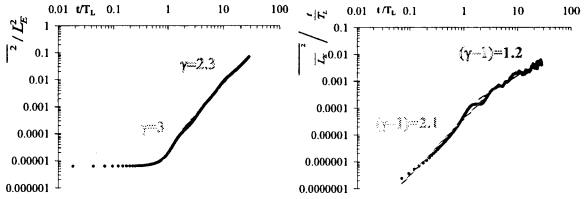

(a) (b)

Figure 11: Two fluid elements dispersion versus t/T_L *(a)* $\overline{(\Delta_{two}/L_E)^2}$; *(b)* $\partial\overline{(\Delta_{two}/L_E)^2}/\partial(t/T_L)$. (1 129 161 pairs)

The exponent of 3.1 obtained for γ during the transient is close to the value of 3 given by the Richardson-Obukhov law for turbulent flows, (Richardson (1926), Obukhov (1941)) even thought our flow is laminar ($Re_{3D} \sim 10$). This exponent has been observed in many experiments (e.g. Julien et al.(1999), Ott & Mann (2000)) and numerical simulations (e.g. Boffeta and Sokolov (2002)). After the transient, the two-particle dispersion shows an exponent of about 2.3. This is higher than the value 2 which could be expected for a simple laminar-shear stretching.

It should be noticed that the root mean square separation of two-fluid elements stays smaller than the integral scale, L_E, of the flow which is about 10 times smaller than the size of the tank. The second regime observed after the transient is self-consistent and does not come from a limiting length reached during dispersion (L_E or $L_{tank}/2$) as might be the case in Julien et al (1999) for the second regime observed but not commented.

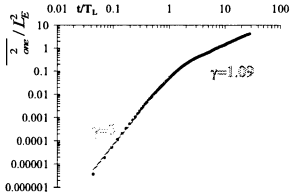

Figure 12: One fluid element dispersion, $\overline{(\Delta_{one}/L_E)^2}$, versus t/T_L. (1 129 161 elements)

Figure 12 gives satistics of one fluid element dispersion. The influence of the energy transient gives a first power law with $\overline{(\Delta_{one}/L_E)^2} \sim (t/T_L)^3$. Once the flow is quasi-stationary $\overline{(\Delta_{one}/L_E)^2} \sim (t/T_L)^{1.1}$ could indicate a random motion. Nevertheless, two-particle statistics remain correlated (for long time) with an exponent clearly different from 1 ($\gamma > 2$). This difference between one- and two- fluid-element(s) dispersion is attributed to the symmetries and numerous time periodicity of the flow: most of the fluid element pairs are trapped in the same quarter of the flow (and

secondary flow structures) while the statistic of one-fluid element dispersion are realized over the four quarters and all secondary flow structures.

Concerning transient effects, Figure 13a shows a linear evolution of the energy with time: $u^2_{rms} \sim t$ for $0 < t \lesssim T_L/2$. The energy growth could also be interpolated using $u^2_{rms} = u^2_\infty(1 - exp(-at\nu/H^2))$ to add the long time asymptote, (cf. Paret et al. (1997)). $u^2_{rms} \sim t$ is in perfect agreement with $\overline{(\Delta_{one}/L_E)^2} \sim (t/T_L)^3$.

The transient corresponds to a step of forcing giving an acceleration to the flow which contributes to fluid element-pair dispersion as it does for one fluid element dispersion. In this case this constant gives $\overline{\Delta^n} \sim t^{3n/2}$. Figure 13b is a comparison of fluid element pair dispersion with the one expected from the constant acceleration effect. The two dispersions are extremely close.

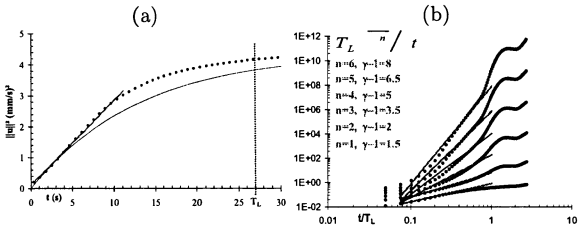

Figure 13: (a) Energy growth during transient. The line corresponds to $u^2_{rms} = u^2_\infty(1 - exp(-at\nu/H^2))$ with a=1.46; (b) $\overline{\Delta^n}$ during the energy transient. The straight lines show the ballistic dispersion associated to accelerated flow for each order. (1 129 161 pairs)

This indicates that the time dependency of the forcing intensity (for EM forced shallow layer) is affecting particle statistics by time dependent "quasi-constant accelerations" and energy transfers (due to bottom friction) associated to a sudden step of EM forcing.

For fluid element statistics realized and started when the flow has reached quasi-stationary state (no energy transient), measurement of one fluid element statistics gives to $\overline{(\Delta_{one}/L_E)^2} \sim (t/T_L)^2$ for $t < L_E/u_{rms}$ which is clearly different from the value of 3 obtained with the additional sudden starting step effect. When $t > L_E/u_{rms}$ $\overline{(\Delta_{one}/L_E)^2} \sim (t/T_L)^1$. Two fluid elements dispersion has an exponential growth for $t < T_L$ and $\overline{(\Delta/L_E)^2} \sim (t/T_L)^{2.5}$ for $t > T_L$.

WORK IN PROGRESS

A variety of avenues are currently being developped. Many types of time-dependent forcing are being considered in the laboratory and in the DNS. Direct Lagrangian measurements are currently being made by Particle Tracking Velocimetry (PTV). Similar fractal forcing schemes over much wider ranges of scales will be studied by DNS. We plan to examine, among other issues, the relation between the Lagrangian exponent, γ, and the Eulerian geometrical exponent, D_s, as well as between the Lagrangian bulk constant, G_Δ, and the Eulerian bulk constant, C_s. These dimensionless numbers control the intensity of concentration fluctuations.

ACKNOWLEDGEMENTS

We want to thank Dimitrios Kolokotronis (Imperial College London) and support from the Leverhulme trust, EPSRC and the Royal Society.

REFERENCES

Boffeta, G., Sokolov, I.M., 2002, "Relative Dispersion in Fully Developed Turbulence: The Richardson's Law and Intermittency Corrections", Phys. Rev. Lett. 88 (9), 094501.

Cardoso, O., Marteau, D., Tabeling, P., 1994, "Quantitative experimental study of the free decay of quasi-two-dimensional turbulence", Physical review E 49, number 1 pp454-461.

Ciofalo, M., 1994, "Large-eddy simulation: a critical survey of models and applications", Adv Heat Transfer 25, 321-419.

Clercx, H.J.H., van Heijst, G.J.F.,Zoeteweij, M.L. , 2003, "Quasi-two-dimensional turbulence in shallow fluid layers: the role of bottom friction and fluid layer depth", Phys. Rev. E 67, 066303.

Davila, J., Vassilicos, J. C., 2003, "Richardson pair diffusion and the stagnation point structure of turbulence", Phys. Rev. Lett. 91 (14), 144501.

Durbin., P.A, 1980, "A stochastic model of two-particle dispersion and concentration fluctuations in homogeneous turbulence", J. Fluid. Mech. 100, 279-302.

Flohr, P., Vassilicos, J.C., 2000, "Scalar subgrid model with flow structure for large-eddy simulation of scalar variances". J. Fluid Mech. 407: 315-349

Fung, J.C.H., Vassilicos, J.C., 1998, "Two-particle dispersion in turbulent like flows", Phys. Rev. E, 57(2):1677-1690.

Goto, S., Vassilicos, J.C., 2004, "Particle pair diffusion and streamline topology in two-dimensional turbulence", New J. Phys. 6, 65.

Hurst, D., Vassilicos, J.C., 2004, "Experiments in fractal induced turbulence", E.T.C. 10 pp355-358.

Julien, M.C., Paret, J., Tabeling, P., 1999, "Richardson Pair Dispersion in Two-Dimensional Turbulence", *Phys. Rev. Lett.*, **82** (14), 2872-2875.

Nicolleau, F., Vassilicos J.C., 2003, "Turbulent Pair Diffusion", *Phys. Rev. Lett.* **90** (2), 024503.

Obukhov, A.M., 1941, "Spectral energy distribution in turbulent flow", *Izv. Akad. Nauk SSSR*, vol **5**,453-566.

Ott, S., Mann J., 2000, "An experimental investigation of the relative diffusion of particles pairs in three-dimensional turbulent flow", *J. Fluid Mech.*, vol **422**,207-223.

Paret, J., Marteau, D., Paireau, O., Tabeling, P., 1997, "Are flows electromagnetically forced in thin stratified layers two-dimensional?", *Phys. Fluids*, **9** (10), 3102-3104.

Queiros-Conde, D., Vassilicos,J.C., 2001, "Turbulent wakes of 3D Fractal Grids", Intermittency in turbulent flows, edited by J.C. Vassilicos, Cambridge University Press.

Richardson, L.F., 1926, "Atmospheric Diffusion Shown on a distance-Neighbour Graph", *Proc. Roy. Soc. London A*, **110** 709-737.

Satijn, M.P., Cense, A.W. , Verzicco,R. , Clercx, H.J.H., Van Heijst, G.J.F. , 2001, "Three dimensional structure and decay properties of vortices in shallow fluid layers", Physics of fluids vol. 13 (7) pp 1932-1945.

Sommeria, J., 1986, "Experimental study of the two-dimensional inverse energy cascade in a square box", J. Fluid Mech., vol 170, pp139-168.

Williams, B.S., Marteau, D. , Gollub, J.P., 1997, "Mixing of a passive scalar in magnetically forced two-dimensional turbulence", Phys. Fluids 9 (7) pp 2061-2080.

Staicu, A., Mazzi, B., Vassilicos, J.C. , van de Water, W., 2003, "Turbulent wakes of fractal objects", Physical Review E, 67, 066306